Derivation and Comparison of SAR and Frequency-Wavenumber Migration Within a Common Inverse Scalar Wave Problem Formulation

Colin Gilmore, *Student Member, IEEE*, Ian Jeffrey, *Student Member, IEEE*, and Joe LoVetri, *Member, IEEE*

***Abstract*—Two common Fourier imaging algorithms used in ground penetrating radar (GPR), synthetic aperture radar (SAR), and frequency-wavenumber (F-K) migration, are reviewed and compared from a theoretical perspective. The two algorithms, while arising from seemingly different physical models: a point-scatterer model for SAR and the exploding source model for F-K migration, result in similar imaging equations. Both algorithms are derived from an integral equation formulation of the inverse scalar wave problem, which allows a clear understanding of the approximations being made in each algorithm and allows a direct comparison. This derivation brings out the similarities of the two techniques which are hidden by the traditional formulations based on physical scattering models. The comparison shows that the approximations required to derive each technique from the integral equation formulation of the inverse problem are nearly identical, and hence the two imaging algorithms and physical models are making similar assumptions about the solution to the inverse problem, thus clarifying why the imaging equations are so similar. Sample images of landmine-like targets buried in sand are obtained from experimental GPR data using both algorithms.**

***Index Terms*—Frequency-wavenumber (F-K) migration, ground penetrating radar (GPR), inverse wave problem, synthetic aperture radar (SAR).**

I. Introduction

In MANY disciplines throughout science and engineering, it is desirable to produce images of both the internal and external structure of remote objects through noninvasive means. Examples of different techniques which have been developed include seismic imaging algorithms used in geophysics [1]–[3], synthetic aperture radar (SAR) [4], X-ray tomography [5], diffraction tomography [6], [7], and magnetic resonance imaging (MRI) [8]. Essential to all these imaging techniques, with the possible exception of MRI, is the use of the scalar wave equation to model the electromagnetic or acoustic fields and the subsequent, explicit or implicit, inversion of that equation. Although a rigorous derivation from the governing equations of the physics is possible (for SAR see, e.g., [9]), these methods usually assume some type of a physical/signal model and derive imaging equations from this [1], [4]. The use of different physical and signal models for deriving these imaging techniques can lead to confusion about the assumptions and mathematical approximations underlying these algorithms.

Each of these imaging techniques identify the unknown image profile (or objective function) as the inverse Fourier Transform of some composite function constructed from the received data signals. The term Fourier imaging is sometimes used to describe imaging algorithms of this type [10]. Often the steps and assumptions required to obtain such a Fourier imaging formulation seem quite dissimilar.

The main goal of this paper is to consider together two seemingly different Fourier imaging techniques and clarify the similarities and differences that exist between them. In particular, we consider two Fourier imaging techniques as applied to the ground penetrating radar (GPR) problem: from the geophysics community, frequency-wavenumber (F–K) migration and, from the radar community, SAR. Both algorithms arise from different physical and signal models, yet yield surprisingly similar Fourier imaging algorithms. The similarities and differences of these algorithms are more easily delineated by formulating both algorithms under a common integral equation representation of the scalar inverse problem as compared to their traditional derivations.

The organization of this paper is as follows. In Section II, we give the required background information on the inverse problem being considered followed in Section III which first outlines the basic SAR imaging algorithm and then shows how to derive the same equation from the full integral formulation of the inverse problem. In Section IV, we first explain the exploding source model, and then we outline and analyze the F-K migration algorithm. In Section V we compare the two algorithms and give representative results of applying them to the imaging of landmine-like targets buried in sand. These images are obtained from experimental GPR data collected using a stepped-frequency radar in a laboratory environment. Finally, in Section VI we give a brief conclusion.

II. Background

Fourier imaging type techniques can be formulated for various physical modalities of interrogating a region of interest, e.g., ultrasound and electromagnetics, but the main feature that allows the methods to be so formulated is the propagation of waves. Mathematically, the effect which is essential to the method is the variation of the speed of propagation throughout the imaging region from which one can infer the dielectric properties of the region. Under different physical modalities the variation in speed of the wave associated with that modality

Manuscript received October 28, 2005; revised December 13, 2005. This work was supported in part by the Natural Sciences and Engineering Research Council of Canada.

The authors are with the Department of Electrical and Computer Engineering, University of Manitoba, Winnipeg, MB R3T 5V6, Canada (e-mail: lovetri@ee.umanitoba.ca).

Digital Object Identifier 10.1109/TGRS.2006.870402

will indicate the variation of a different physical material parameter. If the variation in speed is attributable to more than one material parameter, e.g., variation in both permittivity and permeability, then there will be an ambiguity in the material parameter corresponding to the resulting Fourier image.

A. Scalar Inverse Problem

Quite arbitrarily, we suppose that one is interested in imaging the dielectric properties of a region using electromagnetic interrogation and that the dielectric properties are the only properties which vary in the imaging region. Electromagnetic field problems are properly formulated using Maxwell's equations but the use of the full vector equations does not yield simple mathematical solutions to the inverse problem. However, under the assumption of slowly varying permittivity with respect to the smallest wavelength being used, Maxwell's equations can be cast into six independent scalar wave equations (one for each rectangular component of the electric and magnetic fields) [5]. Assuming that the radar transmits and receives only one rectangular electric field component, and that the dielectric inhomogeneity of the region does not affect the polarization, we can utilize a scalar wave equation model for the inverse problem. With these assumptions, we can write the scalar wave equation governing the particular field component we're interested in as

$$\nabla^2 u(\bar{r},t) - c^{-2}(\bar{r})\partial_t^2 u(\bar{r},t) = -S(\bar{r},t) \tag{1}$$

where $u(\bar{r},t)$ is the scalar wave field, $c(\bar{r})$ is the speed of propagation in the medium, and $S(\bar{r},t)$ is a source term.

In what follows, we assume an $e^{j\omega t}$ time-harmonic dependence for all fields and separate the total field into incident, $u^i(\cdot)$, and scattered, $u^s(\cdot)$, field components. The wave equation can be converted into an equivalent integral equation formulation referred to as the *domain equation* with $\bar{r} \in D$

$$u(\bar{r},\omega) = u^i(\bar{r};\omega) + \omega^2 \int_D G(\bar{r},\bar{r}';\omega) O(\bar{r}') u(\bar{r}';\omega)\, d\bar{r}' \tag{2}$$

where $G(\bar{r},\bar{r}';\omega)$ is the free-space Green's function, $O(\bar{r}) \triangleq (c(\bar{r})^{-2} - c_0^{-2})$ is defined as the objective or contrast function, $u(\bar{r};\omega)$ is the total field, D is the imaging domain, $c(\bar{r})$ is the speed of wave propagation in D, and c_0 is the background velocity of wave propagation. We are free to pick D to suit our particular problem, as long as it contains all regions where $O(\bar{r})$ is nonzero.

The inverse problem for the scalar wave equation can be stated as: Given the scattered field, $u^s(\bar{r};\omega)$, at some observation points, $\bar{r}$, outside the imaging region, recover the objective function $O(\bar{r}')$. Mathematically, this means that we must solve the *data equation* with $\bar{r} \notin D$ [5], [11]

$$u^s(\bar{r};\omega) = \omega^2 \int_D G(\bar{r},\bar{r}';\omega) O(\bar{r}') u(\bar{r}';\omega)\, d\bar{r}'. \tag{3}$$

Equation (3) is sometimes referred to as the Lipmann-Schwinger Equation. Due to the multiplication of the two unknowns, $O(\bar{r})$ and $u(\bar{r};\omega)$ in the data and domain equations this inverse problem is nonlinear. In addition, for spatial and frequency limited data, the inverse problem is ill-posed (in the sense that the solution is nonunique and small changes in the data may result in arbitrarily large changes in the solution). Thus, in order to achieve efficient solutions to this problem, various simplifying assumptions must be made.

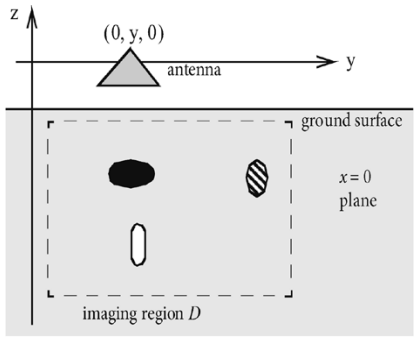

Fig. 1. Physical configuration of imaging problem.

B. Basic Physical Configuration and the 2.5-D Model

The physical configuration considered in this paper is shown in Fig. 1. An antenna located at $\bar{r} = (0, y, 0)$ radiates an incident field into the ground in an attempt to image the medium, i.e., the ground and the inhomogenieties in it. We assume for this paper a monostatic configuration wherein the same antenna both transmits and receives. Data is collected by moving the antenna along the one-dimensional line described by the y axis, although during transmit and receive, we assume that the antenna is static. (This is sometimes referred to as Stripmap SAR [4].) We assume that the reflection from the air–ground interface is part of the scattering process and we are therefore imaging the whole ground (i.e., we use the free-space Green's function, not the half-space Green's function).

The two and one half dimensional (2.5-D) model, which is used in the paper for the analysis of both F-K migration and SAR, consists of the assumption of three-dimensional (3-D) spherical spreading of propagating waves, with a two-dimensional (2-D) variability in the medium to be imaged. In practice, this means the utilization of the 3-D Green's function, with "volume" integrals, such as those in the data (3) and domain (2) equations ranging over two dimensions. This is a commonly used model for this type of imaging [2].

III. SAR Analysis

A. SAR Algorithm

We now present the synthetic aperture radar algorithm as given in [4]. A radar, with an omnidirectional radiation pattern, emits a pulse $p(t)$ from the location $(0, y, 0)$. Assuming a constant velocity of light, c_0 and that the object to be imaged is composed of N point targets in space located at $(0, y_i, z_i)$, each with an associated "reflectivity," $\sigma_i, i = 1 \ldots N$, the received signal is modeled as

$$u(y,t) = \sum_{i=0}^{N-1} \sigma_i p(t - 2c_0^{-1}\sqrt{(y-y_i)^2 + z_i^2}) \tag{4}$$

where the $1/R$ spherical decay term has been ignored. Next, the Fourier Transform (FT) in the time variable is taken, giving the received signal in the frequency domain as

$$u(y,\omega) = P(\omega)\sum_{i=0}^{N-1}\sigma_i e^{-j2k\sqrt{(y-y_i)^2+z_i^2}} \tag{5}$$

where $k=\omega/c_0$ is the usual wave-number and we have utilized (and continue to utilize throughout this paper) the Fourier transform with $e^{j\omega t}$ in the forward transform, and the $1/2\pi$ term in the inverse transform. Next, the Fourier transform is taken with respect to the y variable, giving

$$U(k_y,\omega) = P(\omega)\sum_{i=0}^{N-1}\sigma_i\int e^{-j2k\sqrt{(y-y_i)^2+z_i^2}}e^{jk_y y}\,dy. \tag{6}$$

In order to solve this equation, the method of stationary phase is utilized [4], [12]. Suppressing an amplitude term $e^{-j\pi/4}/\sqrt{4k^2-k_y^2}$ which results from the use of the method of stationary phase, we arrive at

$$\begin{aligned} U(k_y,\omega) &= P(\omega)\sum_{i=0}^{N-1}\sigma_i e^{-jz_i\sqrt{4k^2-k_y^2}-jy_ik_y} \\ &= P(\omega)\sum_{i=0}^{N-1}\sigma_i e^{-jz_i\sqrt{4\frac{\omega}{c_0^2}-k_y^2}-jy_ik_y}. \end{aligned} \tag{7}$$

If we define our "ideal image" to be a series of Dirac delta functions scaled by the reflectivity, i.e.,

$$g(y,z) = \sum_{i=0}^{N-1}\sigma_i\delta(y-y_i, z-z_i) \tag{8a}$$

and note that the phase term of the SAR signal is now linear in y_i and z_i, we can make the observation that the two-dimensional Fourier transform in the y and z variables of our "ideal" image, $g(y,z)$, is equal to the SAR signal in the k_y and ω domains, given by (7), divided by the Fourier transform of the transmitted pulse, i.e.,

$$G(k_y,k_z) = \frac{U(k_y,\omega)}{P(\omega)} \tag{8b}$$

where we must make use of the spatial-frequency mapping equation

$$k_z = \sqrt{4(\omega^2\backslash c_0^2)-k_y^2} \tag{9}$$

to relate values of $U(k_y,\omega)$ and $P(\omega)$ at ω to values of $G(k_y,k_z)$ at k_z. The final SAR imaging equation can be written as

$$\begin{aligned} g(y,z) = \frac{1}{(2\pi)^2}\int\int &\frac{U(k_y,\omega(k_z))}{P(\omega(k_z))} \\ &\times e^{-jk_y y-jk_z z}\,dk_y\,dk_z. \end{aligned} \tag{10}$$

In the practical implementation of the SAR algorithm, these frequency variables (e.g., ω, k_z) are discrete and the use of the mapping equation creates an interpolation problem. A more detailed account of this interpolation problem is given in [13].

B. Analysis of SAR Algorithm Within the Integral Formulation of the Inverse Problem

The electromagnetic assumptions required for the above SAR derivation are not explicit in the derivation itself. A more rigorous formulation which lays bare the assumptions required from an electromagnetic perspective can be obtained from a solution of the integral formulation of the inverse problem. First, we make the assumption that the second term in the *domain equation*, (2), is zero, i.e.,

$$u(\bar{r};\omega) = u^i(\bar{r};\omega), \qquad \bar{r}\in D. \tag{11}$$

This is known as the Born approximation and is valid for targets with small contrast values. This is equivalent to ignoring multiple scattering within the imaging area [5], [11].

Next, we utilize the so-called 2.5-D model, with the assumption of spherical spreading of the wave (i.e., we use the 3-D Green's function) with 2-D variability in the medium. Thus, the scattered (received) field becomes

$$\begin{aligned} u^s(\bar{r},\omega) = \omega^2\int\int &\frac{e^{-jk|\bar{r}-\bar{r}'|}}{4\pi|\bar{r}-\bar{r}'|} \\ &\times O(y',z')u^i(y',z';\omega)\,dy'\,dz' \end{aligned} \tag{12}$$

where $\bar{r}'=(0,y',z'), \bar{r}\notin D$ and we have selected the free-space Green's function

$$G(\bar{r},\bar{r}';\omega) = \frac{e^{-jk|\bar{r}-\bar{r}'|}}{4\pi|\bar{r}-\bar{r}'|}.$$

The 4π in the denominator will be dropped for the remainder of the paper because it makes no difference to the resulting images.

Assuming, as before, that the objective function consists of N Dirac delta functions scaled by a reflectivity, we write the contrast function as

$$O(y',z') = \sum_{i=0}^{N-1}\sigma_i\delta(y'-y_i, z'-z_i). \tag{13}$$

We now assume that the incident field is of the form

$$u^i(\bar{r};\omega) = P(\omega)e^{-jk|\bar{r}-\bar{r}'|} \tag{14}$$

which represents a family of nondecaying spherical waves centred at the monostatic transmitter/receiver point $\bar{r}$. Using the fact that the scattered field is collected along the line $r=(0,y,0)$, the expression for the received scattered field becomes

$$u^s(0,y,0;\omega) = \omega^2 P(\omega)\sum_{i=0}^{N-1}\sigma_i\frac{e^{-j2k\sqrt{(y-y_i)^2+z_i^2}}}{\sqrt{(y-y_i)^2+z_i^2}}. \tag{15}$$

Ignoring the $1/R$ spreading term which came from the Green's function, as well as the ω^2 term, we get

$$u^s(y;\omega) \cong P(\omega)\sum_{i=0}^{N-1}\sigma_i e^{-j2k\sqrt{(y-y_i)^2+z_i^2}} \tag{16}$$

which is identical to the SAR signal given in (5). The imaging equation for SAR can now be derived from this equation in exactly the same manner as in Section III-A, i.e., by taking the Fourier Transform in the z variable, etc.

Neglect of the $1/R$ term is usually justified because the phase term in the exponential part of (15) is much more important [4]. From a physical point of view, the removal of the ω^2 term from (15) can be viewed in several ways. The first is that the removal can be seen as an assumption that the signal is narrow-band, and that the square of the frequency does not vary significantly over the radar bandwidth. The other is that the incident field can be approximated by its own second derivative (which is not a good approximation in most cases). In fact, the ω^2 term arises because the source term in the wave equation for the scattered field contains a second derivative in time of the total field (details can be found in [5], [11]). Another option which would also eliminate this term would be to assume an incident field of the form

$$u^i(\bar{r};\omega) = \omega^{-2} P(\omega) e^{-jk|\bar{r}-\bar{r}'|}.$$

However, incident fields of this type are not normally generated by radars, and we choose to remain with the initial interpretation of an incident field given in (14).

None of these physical interpretations seem justifiable in themselves. The fact that the ω^2 term is dropped in practice can be better justified by its effect on the resulting imaging (10). If the ω^2 term is retained, the result would be an ω^2 in the denominator of the integrand of (10) and this would low-pass filter the corresponding image by strongly emphasizing contributions from low-frequencies. Images obtained with the ω^2 term in (10) give a better representation of the actual permittivity of the medium but are less useful for purposes of detection. Another way of interpreting the dropping of this term is as performing an edge-detection in the range dimension.

We have shown that the SAR model can be viewed as an approximate inversion of the inverse scattering problem, under the Born approximation and a 2.5-D model, with point scattering targets and the incident field assumed to be a nondecaying point source travelling from the point $\bar{r} = (0, y, 0)$ to each point target. It is important to note that in order to obtain the SAR imaging equation, one additional approximation must be made, in particular the approximation of stationary phase.

IV. Frequency-Wavenumber Migration Analysis

Frequency-Wavenumber (F-K) migration, also known as Stolt migration, was first developed by R.H. Stolt in 1978 [1]. It is based on the exploding source model and can be shown to be equivalent to Kirchhoff migration [3], which is also based on the exploding source model. Thus, the following analysis of F–K migration implicitly applies to Kirchhoff migration as well.

A. Exploding Source Model

In the exploding source model, we assume that the scattered field originates from point sources located throughout the imaging region. At time $t = 0$ these sources "explode" and propagate toward the receiver [3], [14]. It is assumed that no interaction occurs between these fictitious point sources which is the same assumption involved in the Born approximation. The use of the exploding source model in seismic imaging and GPR problems consists of two steps.

1) To ensure that the exploding source field arrives at the same time as the actual scattered field, the velocity of propagation in the surrounding medium must be replaced by half its true value.
2) The image in the exploding source model is defined to be the scalar wavefield at time $t = 0$.

Comments on these assumptions are left for Section V-C.

B. Frequency-Wavenumber Migration

For the derivation of F–K migration, we assume the source-free scalar wave equation with constant velocity applies. Here we follow the derivation provided by Scheers [14]. As before, the scattered field data is collected along the y axis: $u^s(0, y, 0; \omega)$. Starting with the source-free 2-D scalar wave equation, (1), and taking the Fourier transform with respect to the y and t variables results in

$$(\partial_z^2 - k_y^2) U(k_y, z, \omega) + \frac{\omega^2}{v^2} U(k_y, z, \omega) = 0 \tag{17}$$

where, as per the assumptions of the exploding source model, $v = c_0/2$. We now define k_z as

$$k_z \triangleq \sqrt{\omega^2 \backslash v^2 - k_y^2} \tag{18}$$

and note that the solution to the differential equation (17) can be written as

$$U(k_y, z, \omega) = A(k_y, \omega) e^{-jk_z} + B(k_y, \omega) e^{jk_z z}. \tag{19}$$

In general, the coefficients $A(k_y, \omega)$ and $B(k_y, \omega)$ need to be obtained from two boundary conditions located at two $z = \text{constant}$ surfaces. However, in typical GPR applications, the field values are obtained only along the $z = 0$ surface, and not even on the whole surface. If an assumption is made that $B(k_y, \omega) = 0$, i.e., we admit only up-coming waves, then we can write the solution to the differential equation in terms of the collected data as

$$U(k_y, z, \omega) = U(k_y, 0, \omega) e^{-jk_z z}. \tag{20}$$

(Note that this is not truly consistent with the idea of exploding sources, as true exploding sources would emit waves in both "up" and "down" directions). After taking the inverse Fourier transform with respect to the and variables, we arrive at

$$u(y, z, t) = \frac{1}{(2\pi)^2} \iint U(k_y, 0, \omega) e^{-jk_y y} e^{-jk_z z} e^{-j\omega t}\, dk_y\, d\omega. \tag{21}$$

Utilizing the second part of the exploding source model, the image is taken to be the scattered field at time $t = 0$. Doing this, and making a switch of coordinates from ω to k_z, we arrive at the final imaging equation

$$\begin{aligned} g(y, z) &\triangleq u(y, z, t)|_{t=0} \\ &= \iint \frac{v^2 \omega(k_z)}{(2\pi)^2 k_z} U(k_y, 0, \omega(k_z)) e^{-jk_y y} e^{-jk_z z}\, dk_y\, dk_z \end{aligned} \tag{22}$$

where we have implicitly made use of the spatial frequency mapping equation, (18), to map values of k_z to values of ω. We

note that because $v = c_0/2$, the mapping equation given in (18) is identical to the mapping equation for SAR, (9), and thus the interpolation problem seen in SAR for practical problems is the same as for F–K migration.

We note here that the two imaging equations, (10) for SAR and (22) for F-K migration are very similar. In particular, for SAR, the imaging procedure consists of taking the Fourier transform of our collected data in the y and t variables, dividing by the magnitude of the transmitted pulse in the frequency domain, interpolating the data collected in ω to k_z, and finally taking the 2-D inverse Fourier transform in the k_y and k_z variables. The process for F–K migration is exactly the same, except that instead of dividing by the magnitude of the pulse in the frequency domain, we multiply the data in the k_y and ω domain by the scale factor $v^2\omega/k_z$ before taking the inverse Fourier transform. It is unclear from this derivation where, if at all, F-K migration takes into account the transmitted pulse characteristics. It is also unclear what the effects of the different scaling terms in the final imaging equations are. The analysis of these issues is left for Section V.

As will be seen in Section V, the differences between images generated by these two algorithms are slight. However, many fundamental questions remain, e.g., Why are the two algorithms so similar despite seemingly different initial models? The problems involved with comparing these two models can be solved by analyzing both under the integral formulation of the inverse problem.

C. Analysis of Frequency-Wavenumber Migration Within the Integral Formulation of the Inverse Problem

F–K migration involves solving the scalar wave equation based on knowledge of the wavefield on the surface $z = 0$ and the assumption that only up-coming waves exist. This solution is completed under the exploding source model where the velocity of light is replaced by half its true value and where the image is taken to be the wavefield at time $t = 0$. Due to the fact that this is a solution of the forward problem, under the exploding source model, the inversion step is actually inside the exploding source model. To properly analyze F–K migration in terms of the integral formulation of the inverse problem we must therefore analyze the exploding source model itself, i.e., we must understand under which conditions does the wavefield at time $t = 0$ accurately model the true objective function, $O(\bar{r})$, in the inverse problem.

We begin by considering the scattered field portion of the domain equation (2)

$$u^s(\bar{r};\omega) = \omega^2 \int_D G(\bar{r},\bar{r}';\omega)O(\bar{r}')u(\bar{r}';\omega)\,d\bar{r}', \qquad \bar{r} \in D. \tag{23}$$

If we assume the Born approximation applies, utilize the free-space Green's function, and assume that the incident field is of the form

$$u^i(\bar{r};\omega) = e^{-jk|\bar{r}-\bar{r}'|} \tag{24}$$

then (23) becomes

$$\begin{aligned} u^s(\bar{r};\omega) &= \omega^2 \int_D G(\bar{r},\bar{r}';\omega)O(\bar{r}')u(\bar{r}';\omega)\,d\bar{r}' \\ &= \omega^2 \int_D O(\bar{r}')\frac{e^{-j2k|\bar{r}-\bar{r}'|}}{|\bar{r}-\bar{r}'|}\,d\bar{r}'. \end{aligned} \tag{25}$$

We now note that (25) is the integral form of the partial differential equation

$$\nabla^2 u^s(\bar{r};\omega) + (2k)^2 u^s(\bar{r};\omega) = -\omega^2 O(\bar{r}). \tag{26}$$

As was done with the analysis of SAR, we now ignore the ω^2 term, and take the inverse Fourier transform with respect to ω, which results in

$$\nabla^2 u^s(\bar{r},t) - v^{-2}\partial_t^2 u^s(\bar{r},t) = -O(\bar{r})\delta(t) \tag{27}$$

where $v = c_0/2$, and $\delta(t)$ is the Dirac delta function. We note that with the use of half the true velocity, this differential equation can be viewed as the differential equation satisfied by the fields generated from the exploding sources, i.e., we have completed the first step of the application of the exploding source model. The term on the right-hand side, $O(\bar{r})\delta(t)$ is equivalent to having an initial condition of $u^s(\bar{r},t)|_{t=0} = O(\bar{r})$ (this can be shown through the use of the Laplace transform). The removal of the ω^2 term from (26) can be viewed in the same manner as was done for the SAR derivation in Section III-B.

The time-domain PDE, (27), has an integral solution of the form

$$u^s(\bar{r},t) = \int\int_D G_0(\bar{r},t|\bar{r}',t)O(\bar{r}')\delta(t')\,d\bar{r}'\,dt' \tag{28}$$

where $G_0(\bar{r},t|\bar{r}',t)$ is the time domain free-space Green's function given by

$$G_0(\bar{r},t|\bar{r}',t) = \frac{1}{|\bar{r}-\bar{r}'|}\delta\left(t - t' - \frac{|\bar{r}-\bar{r}'|}{v}\right). \tag{29}$$

Utilizing the exploding source concept that the image we wish to display is the scattered field at time $t = 0$, we set $t = 0$ in (28) and arrive at

$$g(\bar{r}) \triangleq u^s(\bar{r},0) = \int_D \frac{1}{|\bar{r}-\bar{r}'|}\delta\left(\frac{|\bar{r}-\bar{r}'|}{v}\right)O(\bar{r}')\,d\bar{r}' \tag{30}$$

where we note that for this equation, both $\bar{r}$ and $\bar{r}'$ range over the imaging region D.

We now arrive at a classical problem in electromagnetics and other field theories, namely that the fields at a source are infinite. Thus, defining the image as the scattered field sources at time $t = 0$ leads to an image with singularities in it. In particular, if we examine (30), we note that the Dirac delta function will sift out all points under the integral where $\bar{r} = \bar{r}'$. However, the leading term, $1/|\bar{r}-\bar{r}'|$, is singular at that point.

To circumvent this problem, we assume (in exactly in the same way as was done in the SAR derivation) that we can ignore the $1/R$ decay in the free-space Greens function. If we do this, we may write that

$$g(\bar{r}) \triangleq u^s(\bar{r},t)|_{t=0} = O(\bar{r}). \tag{31}$$

TABLE I
COMPARISON OF ASSUMPTIONS MADE FOR SAR VERSUS F–K MIGRATION

Assumptions made for SAR	Assumptions made for F-K Migration
Incident field of $u^i(\bar{r};\omega) = P(\omega)e^{-j\omega\lvert\bar{r}-\bar{r}'\rvert}$	Incident field of $u^i(\bar{r};\omega) = P(\omega)e^{-j\omega\lvert\bar{r}-\bar{r}'\rvert}$
Born Approximation	Born Approximation
Ignore the ω^2 dependence of the scattered field	Ignore the ω^2 dependence of the scattered field
Ignore the $1/R$ decay in the free-space Green's function	Ignore the $1/R$ decay in the free-space Green's function
Method of stationary phase is applied	Only up-coming waves from the 'exploding sources'

Thus, given the assumptions of the Born approximation, the incident field being that of a nondecaying point source, ignoring the ω^2 term in the right-hand side of (26), and ignoring the $1/R$ spherical spreading, the exploding source model offers an approximate inversion of the scalar form of the inverse problem. Therefore, we can conclude that any imaging algorithm which uses the exploding source model, such as F–K migration, is an approximate inversion under these assumptions.

V. COMPARISON AND ANALYSIS OF SAR AND F–K MIGRATION IMAGING ALGORITHMS

Now that both the SAR and F–K migration algorithms have been analyzed under the integral formulation of the scalar inverse problem, we are able to compare them without the added confusion of seemingly disparate physical models. Both algorithms are an approximate solution to the scalar inverse problem, with a series of assumptions made. The assumptions made for each particular algorithm are shown in Table I. It is important to note that the first four assumptions made in the F–K migration algorithm are implicit in the exploding source model.

Seen in this tabular form, the reasons why the two final imaging equations for SAR and F–K migration are so similar becomes clear—it is because the underlying assumptions made by the imaging algorithms in the solution of the more rigorous inverse problem are almost identical.

In particular, the first four assumptions in Table I are identical (with the exception of the $P(\omega)$ term). Both algorithms assume the Born approximation applies, both assume that the incident field consists of a family of nondecaying spherical waves centered at the receiver point $\bar{r}$, both ignore the ω^2 dependence of the scattered field and both (at the final stages of derivation) ignore the $1/R$ decay of the Green's function. The only major difference comes at the fifth assumption—for SAR the method of stationary phase is used to obtain a Fourier transform type signal, and in F–K migration, it is necessary to assume only up-coming waves from the exploding sources in order to solve the partial differential equation (17) (and thus obtain a Fourier integral solution, with a different scaling factor in the Fourier integral).

The final minor difference between the two algorithms is the amplitude term, $P(\omega)$, in the SAR incident wave which takes into account the amplitude of the transmitted pulse at each frequency. This term is missing in the incident wave of the F–K migration algorithm, but this can easily be introduced into the algorithm.

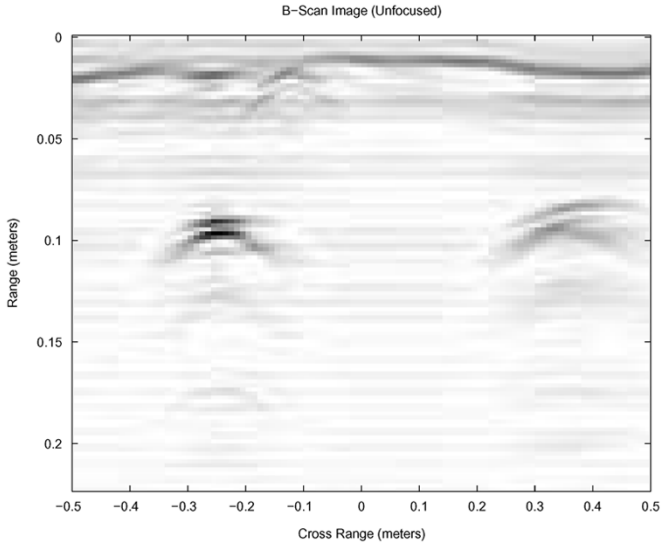

Fig. 2. Unfocused experimental data.

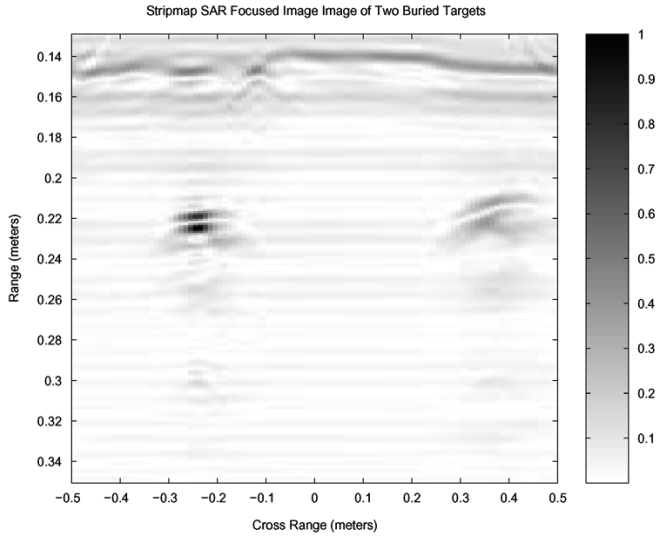

Fig. 3. SAR focused image of two buried targets.

It is important to note that these two algorithms show very few differences with respect to the images generated from both synthetic and experimental data [15]. To illustrate these differences, experimental data were collected in a laboratory sandbox environment. Data were collected using an Anritsu 360 A vector network analyzer (VNA) operating from 1–12.4 GHz. The system uses a monostatic antenna configuration with a double-ridge horn antenna. The forward reflection S-parameter (S11) is utilized as the radar response for subsequent signal processing. The antenna was always directed with maximum power toward the ground. In our laboratory setup, the ground medium was dry silica sand with a dielectric constant of $\varepsilon_r \cong 2.4$. In this experimental setup two landmine-sized targets were buried in the sand approximately 10 cm below the surface. Data were collected in 1 cm cross-range steps, over a total 1-m cross-range.

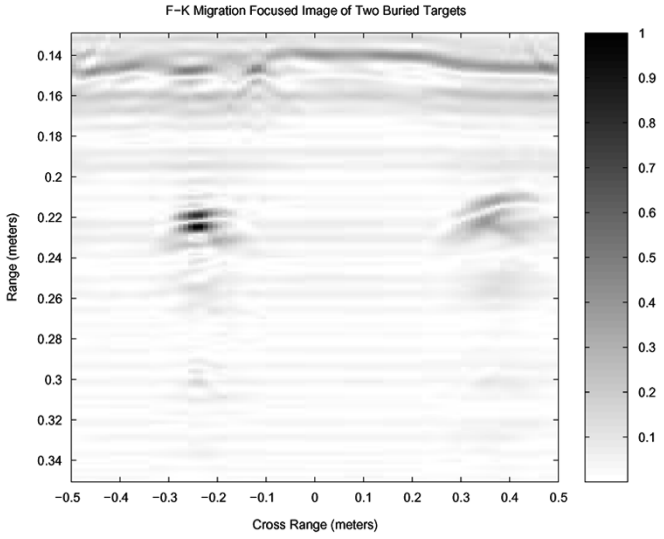

Fig. 4. F–K migration focused image of two buried targets.

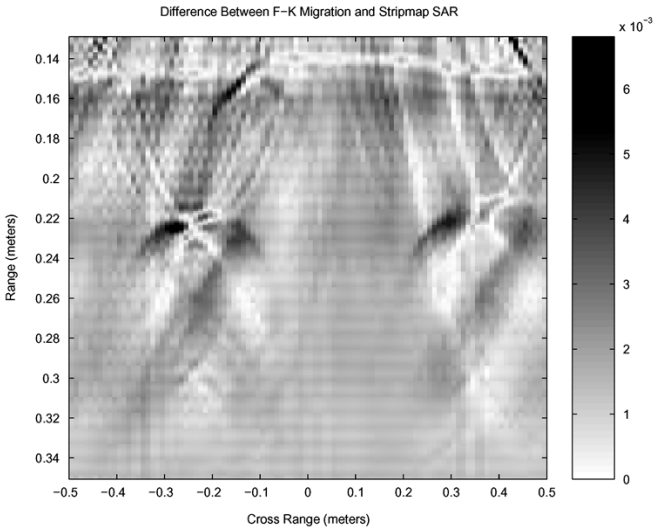

Fig. 5. Difference between F–K migration and SAR focused images of two buried targets.

Fig. 2 shows the unfocused B-scan image, where the two targets and ground surface are clearly visible in the image. Figs. 3 and 4 show the normalized SAR and normalized F–K migration focused images respectively. The reader may note that there is little discernible difference between the two images. Finally, Fig. 5 shows the difference between the normalized F-K migration and normalized SAR images. The magnitude of the differences between the two images is on the order of 10^{-3} below the peak values in the image, thus illustrating that there is very little difference between the algorithms from an imaging perspective.

VI. Conclusion

We have shown how two Fourier imaging techniques arising from different areas: frequency-wavenumber migration, from geophysics, and SAR, from the radar community, are derived. Based on an analysis of both imaging algorithms within the framework of the integral formulation of the scalar inverse problem it has been shown why the two algorithms are so similar and where the differences do occur. Essentially, the two algorithms are identical, with no practical advantage of one over the other.

References

[1] R. Stolt, "Migration by Fourier transform," *Geophys.*, vol. 43, no. 1, pp. 23–48, 1978.
[2] N. Bleistein, J. K. Cohen, and J. W. Stockwell Jr., *Mathematics of Multidimensional Seismic Imaging, Migration and Inversion*. New York: Springer, 2000.
[3] M. S. Zhdanov, *Geophysical Inverse Theory and Regularization Problems*. New York: Elsevier, 2002.
[4] M. Soumekh, *Synthetic Aperture Radar Signal Processing with MATLAB Algorithms*. New York: Wiley, 1999.
[5] M. Born, *Principles of Optics*, 6th ed. Cambridge, U.K.: Cambridge Univ. Press, 1980.
[6] A. J. Devaney, "A filtered backpropagation algorithm for diffraction tomography," *Ultrason. Imag.*, vol. 4, pp. 336–350, 1982.
[7] J. E. Molyneux and A. Witten, "Diffraction tomographic imaging in a monostatic measurement geometry," *IEEE Trans. Geosc. Remote Sens.*, vol. 31, no. 2, pp. 507–511, Mar. 1993.
[8] Z. P. Liang and P. C. Lauterbur, *Principles of Magnetic Resonance Imaging: A Signal Processing Perspective*. New York: Wiley, 1999.
[9] M. Cheney, "A mathematical tutorial on synthetic aperture radar," *SIAM Rev.*, vol. 43, no. 2, pp. 301–312, 2001.
[10] M. Soumekh, *Fourier Array Imaging*. Englewood Cliffs, NJ: Prentice-Hall, 1994.
[11] M. Oristaglio and H. Blok, "Wavefield imaging and inversion in electromagnetics and acoustics," *Course Notes*, 1995.
[12] A. Papoulis, *The Fourier Integral and Its Applications*. New York: McGraw-Hill, 1962.
[13] R. M. Mersereau and A. V. Oppenheim, "Digital reconstruction of multidimensional signals from their projections," in *Proc. IEEE*, vol. 62, Oct. 1974, pp. 1319–1338.
[14] "Ph.D. thesis,", Univ. Catholique de Louvain, Lab. D'Hyperfrequences, Louvain-la-Neuve, Belgium, 2001.
[15] C. Gilmore, I. Jeffrey, H. Su, M. Phelan, and J. LoVetri *et al.*, "Comparison of seismic migration and stripmap SAR imaging methods for GPR landmine detection," in *Ultra-Wideband Short-Pulse Electromagnetics 7*, F. Sabath *et al.*, Eds. Norwell, MA: Kluwer/Plenum, 2006.

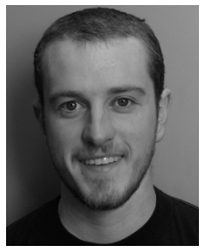

Colin Gilmore (S'05) received the B.Sc. (with distinction and winning the gold medal) and the M.Sc. degrees in electrical engineering from the University of Manitoba, Winnipeg, MB, Canada, in 2002 and 2005, respectively, where he is currently pursuing the Ph.D. degree in electrical engineering.

His current research interests are in the areas of GPR, signal processing, computational electromagnetics, and inverse problems. He held a Canadian Natural Sciences and Engineering Research Council (NSERC) Post-Graduate Scholarship A from 2002 to 2004 and currently holds an NSERC Canada Graduate Scholarship.

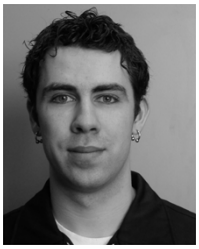

Ian Jeffrey (S'05) received the B.Sc. degree in computer engineering (with distinction) and the M.Sc. degree in electrical and computer engineering from the University of Manitoba, Winnipeg, MB, Canada, in 2002 and 2004, respectively, where he is currently pursuing the Ph.D. degree in electrical and computer engineering.

His current research interests are in the areas of computational electromagnetics, electromagnetic compatibility, and inverse imaging. He held a Canadian NSERC Post-Graduate Scholarship A from 2002 to 2004 and currently holds an NSERC Post-Graduate Scholarship B.

Joe LoVetri (M'91) received the Ph.D. degree in electrical engineering from the University of Ottawa, Ottawa, ON, Canada, in 1991.

From 1991 to 1999, he was an Associate Professor in the Department of Electrical and Computer Engineering, University of Western Ontario, Canada. He is currently a Professor in the Department of Electrical and Computer Engineering, and Associate Dean (Research) of the Faculty of Engineering at the University of Manitoba, Winnipeg, MB, Canada. His main research interests are in time-domain CEM, modeling of EMC problems, GPR, and inverse imaging techniques.